Princeton Plasma Physics Laboratory

PPPL-4031

PPPL-4031

# Implicit Solution of the Four-field Extended-magnetohydrodynamic Equations using High-order High-continuity Finite Elements

S.C. Jardin and J.A. Breslau

December 2004

PPPL
PRINCETON PLASMA
PHYSICS LABORATORY

Prepared for the U.S. Department of Energy under Contract DE-AC02-76CH03073.

# PPPL Report Disclaimers

## Full Legal Disclaimer



## Trademark Disclaimer



# PPPL Report Availability

This report is posted on the U.S. Department of Energy's Princeton Plasma Physics Laboratory Publications and Reports web site in Fiscal Year 2005. The home page for PPPL Reports and Publications is: http://www.pppl.gov/pub_report/

## Office of Scientific and Technical Information (OSTI):

Available electronically at: http://www.osti.gov/bridge.

Available for a processing fee to U.S. Department of Energy and its contractors, in paper from:

U.S. Department of Energy
Office of Scientific and Technical Information
P.O. Box 62
Oak Ridge, TN 37831-0062

Telephone: (865) 576-8401

Fax: (865) 576-5728

E-mail: reports@adonis.osti.gov

## National Technical Information Service (NTIS):

This report is available for sale to the general public from:

U.S. Department of Commerce
National Technical Information Service
5285 Port Royal Road
Springfield, VA 22161

Telephone: (800) 553-6847

Fax: (703) 605-6900

Email: orders@ntis.fedworld.gov

Online ordering: http://www.ntis.gov/ordering.htm

# Implicit solution of the four-field extended-magnetohydrodynamic equations using high-order high-continuity finite elements

**S. C. Jardin and J. A. Breslau**

*Plasma Physics Laboratory, Princeton University, P.O. Box 451, Princeton, NJ 08543*

Revised December 22, 2004

## Abstract

Here we describe a technique for solving the four-field extended-magnetohydrodynamic (MHD) equations in two dimensions. The introduction of triangular high-order finite elements with continuous first derivatives ($C^1$ continuity) leads to a compact representation compatible with direct inversion of the associated sparse matrices. The split semi-implicit method is introduced and used to integrate the equations in time, yielding unconditional stability for arbitrary time step. The method is applied to the cylindrical tilt mode problem with the result that a non-zero value of the collisionless ion skin depth will increase the growth rate of that mode. The effect of this parameter on the reconnection rate and geometry of a Harris equilibrium and on the Taylor reconnection problem is also demonstrated. This method forms the basis for a generalization to a full extended-MHD description of the plasma with six, eight, or more scalar fields.

PACS category: 52.30 Ex
*Keywords:* Magnetohydrodynamics, two-fluid, numerical methods, finite elements

Tel.: +1-609-243-2635
E-mail addresses: jardin@pppl.gov, jardin@princeton.edu (S.C. Jardin)

## I. Introduction

It has been recognized for some time that it is necessary to go beyond the simple "resistive MHD" description of the plasma in order to get the correct quantitative results for the growth and saturation of global dissipative modes in a fusion device. The inclusion of a more complete "generalized Ohms law" and the off-diagonal terms in the ion pressure tensor introduce whistler waves, kinetic Alfvén waves, and gyro-viscous waves, all of which are dispersive and require special numerical treatment. We describe a numerical approach to solving these extended-MHD equations using a compact representation that is specifically designed to yield efficient, high-order-of-accuracy implicit solutions of a general formulation of the extended-MHD equations. The representation is based on a triangular finite element with fifth order accuracy that is constructed to have continuous derivatives across element boundaries. The Galerkin technique allows this element to be applied to systems of equations containing spatial derivative operators of up to fourth order. The final set of discrete block matrix equations is solved using a parallel sparse direct solver.

For the general formulation, the magnetic and velocity fields are decomposed without loss of generality in a potential, stream function form as in [1]. Formulating the problem in these variables allows two non-trivial subsets of equations that can be studied before embarking on the full set of equations. The two-variable system described in [2] is the well known two-field “reduced MHD” equations consisting of a single flux function for the magnetic field and a single stream function for the velocity. The present paper describes the method applied to a more complex subsystem: the four-field reduced MHD equations, also known as the reduced two-fluid MHD equations. This set of equations contains both MHD behavior associated with the shear Alfvén wave and the essential features of the whistler and kinetic

Alfvén wave physics. Variations of these equations have been extensively studied in the literature [3-5].

We present the four-field equations in Sec. II, and then describe the split semi-implicit method for their solution in Sec. III and the numerical stability of this method in Sec. IV. Sections V, VI, and VII present applications of this method to three model problems: presenting new results on the effect of the collisionless ion skin depth on the growth rate of the tilt mode in Sec. IV and confirming the importance of this term on reconnection rates in Secs. VI and VII. The paper is summarized with discussion in Sec. VIII.

**II. The Equations**

The reduced two-dimensional (*x*,*y*) two-fluid MHD equations in the limit of zero electron mass can be written [3]

$$\frac{\partial}{\partial t}\nabla^2\phi = \left[\phi, \nabla^2\phi\right] + \left[\nabla^2\psi, \psi\right] + \mu\nabla^4\phi \ , \tag{1a}$$

$$\frac{\partial V_z}{\partial t} = \left[\phi, V_z\right] + \left[I, \psi\right] + \mu\nabla^2 V_z - \mu h\nabla^4 V_z \ , \tag{1b}$$

$$\frac{\partial \psi}{\partial t} = \left[\phi, \psi\right] + d_i\left[\psi, I\right] + \eta\nabla^2\psi - \nu\nabla^4\psi \ , \tag{1c}$$

$$\frac{\partial I}{\partial t} = \left[\phi, I\right] + d_i\left[\nabla^2\psi, \psi\right] + \left[V_z, \psi\right] + \eta\nabla^2 I - \nu\nabla^4 I \ . \tag{1d}$$

Here we have utilized the Poisson bracket notation:

$$\left[a, b\right] \equiv \nabla a \times \nabla b \cdot \hat{z} \ .$$

Here, $\phi$ is the in-plane velocity stream function, $V_z$ is the *z*-component of the velocity, $\psi$ is the magnetic flux function, and *I* is the *z*-component of the magnetic field. Thus, the magnetic field and (incompressible) fluid velocity are represented as: $\vec{B} = \nabla\psi \times \hat{z} + I\hat{z}$

; $\vec{V} = \nabla\phi \times \hat{z} + V_z \hat{z}$ . It is shown in [3] that Eqs. (1a-d) are valid in the low guide-field limit in which whistler waves are the dominant two-fluid effect, but that a very similar set of equations is valid in the high guide-field limit in which the kinetic Alfvén wave is prominent. Thus, we take the Eqs. (1) to be typical of the extended MHD equations in two dimensions.

The fluid viscosity, electrical resistivity, hyper-resistivity (or electron viscosity) and collisionless ion skin depth are given by $\mu$ , $\eta$ , $\nu$ , and $d_i$ . The parameter *h* is a hyper-viscosity coefficient added to damp spurious oscillations that might otherwise develop. Terms involving the electron mass have been neglected. The two-field reduced MHD system studied in [1] are just Equations (1a) and (1c) with the parameter $d_i$ set to zero.

The equations (1) have the energy integral (in the absence of sources):

$$\tfrac{1}{2}\frac{\partial}{\partial t}\iint\left\{|\nabla\phi|^2 + V_z{}^2 + |\nabla\psi|^2 + I^2\right\}dA = -\iint\left\{\begin{array}{l}\mu\left|\nabla^2\phi\right|^2 + \mu\left|\nabla V_z\right|^2 + \eta\left|\nabla^2\psi\right|^2 + \eta\left|\nabla I\right|^2 \\ +\mu h\left|\nabla^2 V_z\right|^2 + \nu\left|\nabla(\nabla^2\psi)\right|^2 + \nu\left|\nabla^2 I\right|^2\end{array}\right\}dA + \oint d\ell\,\hat{n}\bullet\nabla\psi\nabla^2\psi \quad . \quad (2)$$

To derive (2), we have assumed the perturbed variables obey the boundary conditions:

$\tilde{\phi} = \mu\hat{n}\bullet\nabla\tilde{\phi} = \tilde{V}_z = \mu h_1\hat{n}\bullet\nabla\tilde{V}_z = \tilde{\psi} = \nu\nabla^2\tilde{\psi} = \tilde{I} = \nu\hat{n}\bullet\nabla\tilde{I} = 0$ .

**III. The Numerical Method:**

To derive the implicit system, we Taylor expand the RHS of Eq. (1) in time to center the spatial derivatives at the advanced time: $t^{n+\theta} \equiv t^n + \theta\delta t$ , keeping only the terms through first order in the time step $\delta t$ . This gives

$$\nabla^2\dot{\phi} = \left[\phi,\nabla^2\phi\right] + \theta\delta t\left[\dot{\phi},\nabla^2\phi\right] + \theta\delta t\left[\phi,\nabla^2\dot{\phi}\right] + \left[\nabla^2\psi,\psi\right] + \theta\delta t\left[\nabla^2\dot{\psi},\psi\right] + \theta\delta t\left[\nabla^2\psi,\dot{\psi}\right] + \mu\nabla^4\phi + \theta\delta t\mu\nabla^4\dot{\phi} \tag{3a}$$

$$\dot{V}_z = \left[\phi,V_z\right] + \theta\delta t\left[\dot{\phi},V_z\right] + \theta\delta t\left[\phi,\dot{V}_z\right] + \left[I,\psi\right] + \theta\delta t\left[\dot{I},\psi\right] + \theta\delta t\left[I,\dot{\psi}\right] + \mu\nabla^2 V_z + \mu\theta\delta t\nabla^2\dot{V}_z - \mu h\nabla^4 V_z - \mu h\theta\delta t\nabla^4\dot{V}_z \tag{3b}$$

$$\dot{\psi} = \left[\phi,\psi\right] + \theta\delta t\left[\dot{\phi},\psi\right] + \theta\delta t\left[\phi,\dot{\psi}\right] + d_i\left[\psi,I\right] + d_i\theta\delta t\left[\dot{\psi},I\right] + d_i\theta\delta t\left[\psi,\dot{I}\right] + \eta\nabla^2\psi + \eta\theta\delta t\nabla^2\dot{\psi} - \nu\nabla^4\psi - \nu\theta\delta t\nabla^4\dot{\psi} \tag{3c}$$

$$\dot{I} = \left[\phi,I\right] + \theta\delta t\left[\dot{\phi},I\right] + \theta\delta t\left[\phi,\dot{I}\right] + d_i\left[\nabla^2\psi,\psi\right] + d_i\theta\delta t\left[\nabla^2\dot{\psi},\psi\right] + d_i\theta\delta t\left[\nabla^2\psi,\dot{\psi}\right] + \left[V_z,\psi\right] + \theta\delta t\left[\dot{V}_z,\psi\right] + \theta\delta t\left[V_z,\dot{\psi}\right] + \eta\nabla^2 I + \eta\theta\delta t\nabla^2\dot{I} - \nu\nabla^4 I - \nu\theta\delta t\nabla^4\dot{I} \tag{3d}$$

The *split semi-implicit* method consists of using Eqs. (3c) and (3d) , but with the field time derivatives $\dot{\psi}$ and $\dot{I}$ on the right of the equal sign set to zero and ignoring (small) dissipative terms, to eliminate time derivatives $\dot{\psi}$ and $\dot{I}$ from Eqs. (3a) and (3b). This has the effect of isolating the linearized Alfvén wave characteristics in those two equations. Thus, the modified velocity equations become:

$$\nabla^2\dot{\phi} = \left[\phi,\nabla^2\phi\right] + \left[\nabla^2\psi,\psi\right] + \mu\nabla^4\phi + \theta\delta t\left\{\begin{array}{l}\left[\nabla^2\left(\left[\phi,\psi\right] + d_i\left[\psi,I\right]\right),\psi\right] + \left[\nabla^2\psi,\left(\left[\phi,\psi\right] + d_i\left[\psi,I\right]\right)\right] \\ + \left[\dot{\phi},\nabla^2\phi\right] + \left[\phi,\nabla^2\dot{\phi}\right] + \mu\nabla^4\dot{\phi}\end{array}\right\} + (\theta\delta t)^2\left\{\left[\nabla^2\left[\dot{\phi},\psi\right],\psi\right] + \left[\nabla^2\psi,\left[\dot{\phi},\psi\right]\right]\right\}, \tag{3a}'$$

$$\dot{V}_z = \left[\phi,V_z\right] + \left[I,\psi\right] + \mu\nabla^2 V_z - \mu h\nabla^4 V_z + \theta\delta t\left\{\begin{array}{l}\left[\left(\left[\phi,I\right] + d_i\left[\nabla^2\psi,\psi\right] + \left[V_z,\psi\right]\right),\psi\right] \\ + \left[I,\left(\left[\phi,\psi\right] + d_i\left[\psi,I\right]\right)\right] + \left[\dot{\phi},V_z\right] + \left[\phi,\dot{V}_z\right] \\ + \mu\nabla^2\dot{V}_z - \mu h\nabla^4\dot{V}_z\end{array}\right\} + (\theta\delta t)^2\left\{\left[\left(\left[\dot{\phi},I\right] + \left[\dot{V}_z,\psi\right]\right),\psi\right] + \left[I,\left[\dot{\phi},\psi\right]\right]\right\}. \tag{3b}'$$

The system (3a)′ , (3b)′ , (3c) and (3d) is solved each time step as two pairs of equations, with Eqs. (3a)′ and (3b)′ being solved first to obtain the velocity time derivatives $\dot{\phi}$ and $\dot{V}_z$ , and these being substituted into Eqs. (3c) and (3d), which are then solved to obtain the field time derivatives $\dot{\psi}$ and $\dot{I}$ .

The motivation is to form two compact systems that can be efficiently solved each time step using elementary matrix methods. The Courant time step restriction associated with the Alfvén waves is eliminated by the implicit simultaneous solution of (3a)′ and (3b)′ . Since Eqs. (3c) and (3d) contain the mechanism for the whistler waves, at least in the electron MHD (EMD) model [6], these can next be solved implicitly to remove the severe time step restriction associated with the dispersive whistler waves.

A similar technique, but applied to the Alfvén wave only, has been called the "differential approximation" in [7] and [8]. The present treatment differs from those in the time-centering of the variables and in the retention of terms linear in $\delta t$ in the modified equations (3a)′ and (3b)′. However the major difference between this and previous work is in the extension of this technique to the whistler wave through equations (3c) and (3d). The numerical stability of this system is discussed in Sec. IV.

To obtain the discrete matrices, we first finite difference in time, with the notation: $\phi^n(x, y) \equiv \phi(x, y, t^n)$ , with *n* being the time index. If we define the time step $\delta t^n \equiv t^{n+1} - t^n$ then the second order expression for the time derivative, centered

about $t = t^{n+1/2}$, is $\delta t\dot{\phi}(x, y, t^{n+1/2}) \cong \phi^{n+1}(x, y) - \phi^{n}(x, y)$. By making use of the readily verified identity,

$$\nabla^2 [a,b] = [\nabla^2 a, b] + [a, \nabla^2 b] + 2[a_x, b_x] + 2[a_y, b_y], \tag{4}$$

straightforward manipulation gives the following set of equations relating the variables at time level *n+1* to those at time level *n*:

$$\{\nabla^2 - \theta\delta t L_{11}^{1v} - (\theta\delta t)^2 L_{11}^{2v}\}\phi^{n+1} = \{\nabla^2 - \theta\delta t L_{11}^{1v} + \delta t L_{11}^{3v} - \theta(\theta-1)(\delta t)^2 L_{11}^{2v}\}\phi^{n} + \theta(\delta t)^2 R_1^{2v} + \delta t R_1^{1v} \tag{5a}$$

$$\begin{aligned}\{-(\theta\delta t)L_{21}^{1v} - (\theta\delta t)^2 L_{21}^{2v}\}\phi^{n+1} + \{1 - \theta\delta t L_{22}^{1v} - (\theta\delta t)^2 L_{22}^{2v}\}V_z^{n+1} = \\ \{-\theta\delta t L_{21}^{1v} + \delta t L_{21}^{3v} - \theta(\theta-1)(\delta t)^2 L_{21}^{2v}\}\phi^{n} + \{1 - \theta\delta t L_{22}^{1v} + \delta t L_{22}^{3v} - \theta(\theta-1)(\delta t)^2 L_{22}^{2v}\}V_z^{n} \\ + \theta(\delta t)^2 R_2^{2v} + \delta t R_2^{1v}\end{aligned} \tag{5b}$$

$$\{1 - \theta\delta t L_{11}^{1p}\}\psi^{n+1} - \theta\delta t L_{12}^{1p} I^{n+1} = \{1 + (1-\theta)\delta t L_{11}^{1p}\}\psi^{n} - \theta\delta t L_{12}^{1p} I^{n} + \delta t R_1^{1p} \tag{5c}$$

$$-\theta\delta t L_{21}^{1p}\psi^{n+1} + \{1 - \theta\delta t L_{22}^{1p}\} I^{n+1} = -\theta\delta t L_{21}^{1p}\psi^{n} + \{1 + (1-\theta)\delta t L_{22}^{1p}\} I^{n} + \delta t R_2^{1p} \tag{5d}$$

Here, we have defined the operators:

$$\begin{aligned}
L_{11}^{1v}\{\phi^{n+1}\} &= [\phi^{n+1}, \nabla^2\phi] + [\phi, \nabla^2\phi^{n+1}] + \mu\nabla^4\phi^{n+1} \\
L_{11}^{2v}\{\phi^{n+1}\} &= [[\phi^{n+1}, \nabla^2\psi], \psi] + [[\nabla^2\phi^{n+1}, \psi], \psi] + [\nabla^2\psi, [\phi^{n+1}, \psi]] \\
&\quad + 2[[\phi_x^{n+1}, \psi_x], \psi] + 2[[\phi_y^{n+1}, \psi_y], \psi] \\
L_{11}^{3v}\{\phi^{n}\} &= [\phi, \nabla^2\phi] + \mu\nabla^4\phi \\
R_1^{2v} &= d_i[[\nabla^2\psi, I], \psi] + d_i[[\psi, \nabla^2 I], \psi] + d_i[\nabla^2\psi, [\psi, I]] \\
&\quad + 2d_i[[\psi_x, I_x], \psi] + 2d_i[[\psi_y, I_y], \psi] \\
R_1^{1v} &= [\nabla^2\psi, \psi]
\end{aligned} \tag{6a}$$

$$
\begin{aligned}
L_{21}^{1v}\left\{\phi^{n+1}\right\} &= \left[\phi^{n+1}, V_z\right] \\
L_{21}^{2v}\left\{\phi^{n+1}\right\} &= \left[\left[\phi^{n+1}, I\right], \psi\right] + \left[I, \left[\phi^{n+1}, \psi\right]\right] \\
L_{22}^{1v}\left\{V_z^{n+1}\right\} &= \left[\phi, V_z^{n+1}\right] + \mu\nabla^2 V_z^{n+1} \\
L_{22}^{2v}\left\{V_z^{n+1}\right\} &= \left[\left[V_z^{n+1}, \psi\right], \psi\right] \\
L_{21}^{3v}\left\{\phi^{n}\right\} &= \tfrac{1}{2}\left[\phi, V_z\right] \\
L_{22}^{3v}\left\{V_z^{n}\right\} &= \tfrac{1}{2}\left[\phi, V_z\right] + \mu\nabla^2 V_z - \mu h\nabla^4 V_z \\
R_2^{2v} &= d_i\left[\left[\nabla^2\psi, \psi\right], \psi\right] + d_i\left[I, \left[\psi, I\right]\right] \\
R_2^{1v} &= \left[I, \psi\right]
\end{aligned}
\tag{6b}
$$

$$
\begin{aligned}
L_{11}^{1p}\left\{\psi^{n+1}\right\} &= \left[\phi, \psi^{n+1}\right] + d_i\left[\psi^{n+1}, I\right] + \eta\nabla^2\psi^{n+1} - \nu\nabla^4\psi^{n+1} \\
L_{12}^{1p}\left\{I^{n+1}\right\} &= d_i\left[\psi, I^{n+1}\right] \\
R_1^{1p} &= \theta\left[\phi^{n+1} - \phi^{n}, \psi\right] \\
L_{21}^{1p}\left\{\psi^{n+1}\right\} &= d_i\left[\nabla^2\psi^{n+1}, \psi\right] + d_i\left[\nabla^2\psi, \psi^{n+1}\right] + \left[V_z, \psi^{n+1}\right] \\
L_{22}^{1p}\left\{I^{n+1}\right\} &= \left[\phi, I^{n+1}\right] + \eta\nabla^2 I^{n+1} - \nu\nabla^4 I^{n+1} \\
R_2^{1p} &= +\theta\left\{\left[\phi^{n+1} - \phi^{n}, I\right] + \left[V_z^{n+1} - V_z^{n}, \psi\right]\right\} + d_i\left[\nabla^2\psi, \psi\right] + \left[V_z, \psi\right]
\end{aligned}
\tag{6c}
$$

We next represent each of the unknown scalar fields as a set of time-varying amplitudes multiplying time-independent spatial basis functions [2]. The domain is divided into *M* triangular regions. Within each triangle *m*, 18 basis functions are defined, $\left\{\nu_{m,i}(x,y); i = 1,18\right\}$ with the properties: (i) each of the basis functions is a quintic polynomial in (*x*,*y*) that has the value unity at one node for either the function or one of its first five derivatives, (ii) the basis function and its first five derivatives are zero at the two other nodes, and (iii) the quintic terms in the polynomial are constrained so that the normal derivative of the basis function is at most a cubic function along each side of the triangle. These conditions are enough to uniquely determine the 21 polynomial coefficients for each basis function and to insure that any scalar field represented in terms of these basis functions will be continuous and have continuous first derivatives across triangle boundaries. This continuity property is denoted in the literature by $C^1$ [9]. Since the basis functions are

capable of representing a complete quartic polynomial, it follows from a Taylor's series expansion that the error should go like $h^5$, where $h$ is a typical size of a triangle.

Using these basis functions, the unknown quantities take the physical significance of being the function, its two first, and three second derivatives at each of the nodes. For example, the stream function is represented as a sum over each of the 18 basis functions in each of the $M$ triangles:

$$\phi^n(x,y) = \sum_{m=1}^{M}\sum_{i=1}^{18} \nu_{m;i}(x,y)\Phi^n_{m;i} \tag{7}$$

The unknowns $\left\{\Phi^n_i; i = 1,18\right\}$ for triangle $m$ break into three sets of six: $\left\{\Phi^n_{m,i}; i = 1,6\right\}$ correspond to $\phi, \phi_x, \phi_y, \phi_{xx}, \phi_{xy}, \phi_{yy}$ at the first node, $\left\{\Phi^n_{m,i}; i = 7,12\right\}$ are the same quantities at the second node, and $\left\{\Phi^n_{m,i}; i = 13,18\right\}$ are these quantities at the third node. Note that all the unknowns in Eq. (7) are located at the nodes and are thus shared with all triangles using that node. Since there are asymptotically an average of six triangles utilizing each node, there are approximately a total of $3\times M$ unknowns for the global representation of each scalar field, rather than $18\times M$, which might be inferred from Eq. (7).

The discrete expansion (7) for each of the four scalar fields is substituted into the four equations (5). The Galerkin method consists of multiplying each equation (5a)-(5d) by each of the basis functions (or trial functions) and integrating these over the domain to obtain matrix equations for the discrete unknowns. Integration by parts is used to shift derivatives onto the trial functions so that no higher than second spatial derivatives appear in the final

integrals. These are allowable in this procedure since the basis functions were constructed to have continuous first derivatives across triangle boundaries.

We next represent each quantity as the sum of an equilibrium part that is independent of time and a perturbed part, thus $\Phi^n \rightarrow \Phi^0 + \Phi^n$, etc. This yields the two sets of matrix equations that can be solved sequentially**:**

$$\begin{bmatrix} S_{11}^{v} & 0 \\ S_{21}^{v} & S_{22}^{v} \end{bmatrix} \begin{bmatrix} \Phi_{m;i}^{n+1} \\ V_{zm,i}^{n+1} \end{bmatrix} = \begin{bmatrix} D_{11}^{v} & 0 \\ D_{21}^{v} & D_{22}^{v} \end{bmatrix} \begin{bmatrix} \Phi_{m;i}^{n} \\ V_{zm,i}^{n} \end{bmatrix} + \begin{bmatrix} R_{11}^{v} & R_{12}^{v} \\ R_{21}^{v} & R_{22}^{v} \end{bmatrix} \begin{bmatrix} \Psi_{m;i}^{n} \\ I_{m,i}^{n} \end{bmatrix} \tag{8}$$

$$\begin{bmatrix} S_{11}^{p} & S_{12}^{p} \\ S_{21}^{p} & S_{22}^{p} \end{bmatrix} \begin{bmatrix} \Psi_{m;i}^{n+1} \\ I_{zm,i}^{n+1} \end{bmatrix} = \begin{bmatrix} D_{11}^{p} & D_{12}^{p} \\ D_{21}^{p} & D_{22}^{p} \end{bmatrix} \begin{bmatrix} \Psi_{m;i}^{n} \\ I_{zm,i}^{n} \end{bmatrix} + \begin{bmatrix} R_{11}^{p} & 0 \\ R_{21}^{p} & R_{22}^{p} \end{bmatrix} \begin{bmatrix} \Phi_{m;i}^{n+1} \\ V_{zm,i}^{n+1} \end{bmatrix} + \begin{bmatrix} Q_{11}^{p} & 0 \\ Q_{21}^{p} & Q_{22}^{p} \end{bmatrix} \begin{bmatrix} \Phi_{m;i}^{n} \\ V_{zm,i}^{n} \end{bmatrix} \tag{9}$$

The block matrix elements appearing here are defined in Appendix B. The matrix equations (8) and (9) are solved sequentially using the distributed version of the direct sparse matrix software package SuperLU [10]. This solution procedure is exceptionally efficient for a linear system, since only a one-time LU decomposition of the two matrices appearing on the left of the equals sign is required. A nonlinear problem requires performing the LU decomposition whenever there is significant change in the values of the matrix elements.

**IV. Numerical Stability**

The split semi-implicit time advance method given by equations (8) and (9) is based on advancing the velocity variables first each time step, followed by advancing the field variables. This clearly leads to a more efficient numerical method than if the coupled system were advanced together, since the rank of each matrix appearing on the left in Eq. (9) is half of what it would be for the combined system. To understand how this leads to an unconditionally stable time advance, let us consider a simpler problem that has the essential features of the one under investigation.

Consider the simplified Hall MHD system for the fluid velocity, $\vec{V}$, the perturbed magnetic field, $\vec{B}$, and the perturbed current density, $\vec{J} = \nabla \times \vec{B}$. Assume for simplicity that the equilibrium magnetic field is uniform and in the $\hat{z}$ direction, and that the density is spatially constant. In suitably normalized units, the linearized momentum equation and the curl of the induction equation become simply:

$$\frac{\partial \vec{V}}{\partial t} = \vec{J} \times \vec{B}_0 \tag{10a}$$

$$\frac{\partial \vec{J}}{\partial t} = \nabla \times \frac{\partial \vec{B}}{\partial t} = \nabla \times \nabla \times \left[ (\vec{V} - d_i \vec{J}) \times \vec{B}_0 \right] \tag{10b}$$

Setting $\vec{B}_0 = \hat{z}$, and specializing for simplicity to wave propagation in the $\hat{z}$ direction so that $\nabla \to \hat{z} \frac{\partial}{\partial z} \equiv \hat{z} \partial_z$, and both $\vec{J}$ and $\vec{V}$ are in the $\hat{x} - \hat{y}$ plane, the split semi-implicit time advance corresponding to equations (5) is

$$\left[ 1 - (\theta \delta t)^2 \nabla^2 \right] (\vec{V}^{n+1} - \vec{V}^n) = \delta t \left\{ \theta \delta t \left[ \nabla^2 \vec{V}^n - d_i \nabla^2 \vec{J}^n \right] \right\} - \delta t \hat{z} \times \vec{J}^n \tag{11a}$$

$$\left[1+\theta\delta t d_i \hat{z}\times\nabla^2\right](\vec{J}^{n+1}-\vec{J}^{n}) = \delta t\hat{z}\times\nabla^2[\theta\vec{V}^{n+1}+(1-\theta)\vec{V}^{n}] - \delta t d_i \hat{z}\times\nabla^2\vec{J}^{n} \tag{11b}$$

Or, in matrix component form:

$$\begin{aligned}
&\begin{bmatrix} 1-(\theta\delta t)^2\partial_z^2 & 0 & 0 & 0 \\ 0 & 1-(\theta\delta t)^2\partial_z^2 & 0 & 0 \\ 0 & \theta\delta t\partial_z^2 & 1 & -\theta\delta t d_i\partial_z^2 \\ -\theta\delta t\partial_z^2 & 0 & \theta\delta t d_i\partial_z^2 & 1 \end{bmatrix} \bullet \begin{bmatrix} V_x \\ V_y \\ J_x \\ J_y \end{bmatrix}^{n+1} \\
&= \begin{bmatrix} 1-\theta(\theta-1)(\delta t)^2\partial_z^2 & 0 & -\theta(\delta t)^2 d_i\partial_z^2 & \delta t \\ 0 & 1-\theta(\theta-1)(\delta t)^2\partial_z^2 & -\delta t & -\theta(\delta t)^2 d_i\partial_z^2 \\ 0 & (\theta-1)\delta t\partial_z^2 & 1 & -(\theta-1)\delta t d_i\partial_z^2 \\ -(\theta-1)\delta t\partial_z^2 & 0 & (\theta-1)\delta t d_i\partial_z^2 & 1 \end{bmatrix} \bullet \begin{bmatrix} V_x \\ V_y \\ J_x \\ J_y \end{bmatrix}^{n}
\end{aligned} \tag{12}$$

The numerical stability is determined by replacing the spatial derivative by an effective wave number, $\nabla^2 = \partial_z^2 \to -k_{eff}^2$ , and by introducing the amplification factor *r* for the vector in Eq. (12). The amplification factor is thus determined by the generalized eigenvalue equation

$$\det\begin{bmatrix} 1-r+\theta(\delta t)^2 k_{eff}^2 s & 0 & \theta(\delta t)^2 d_i k_{eff}^2 & \delta t \\ 0 & 1-r+\theta(\delta t)^2 k_{eff}^2 s & -\delta t & \theta(\delta t)^2 d_i k_{eff}^2 \\ 0 & -\delta t k_{eff}^2 s & -r & -d_i\delta t k_{eff}^2 s \\ \delta t k_{eff}^2 s & 0 & -d_i\delta t k_{eff}^2 s & -r \end{bmatrix} = 0 \quad , \tag{13}$$

with $s \equiv \left[(1-r)\theta - 1\right]$. Evaluation of Eq. (13) with both a generalized eigenvalue solver and by symbolic expansion of the determinant and using a polynomial root finder give identical results: the amplification factor $|r| \le 1$, and thus the system is stable, for arbitrary real $k_{eff}^2 > 0$ , $\delta t > 0$, and $d_i > 0$ provided the implicit parameter satisfies $\theta \ge 1/2$.

## V. The Tilting Cylinder

Here we apply the method to an extension of the analysis of the tilting cylinder problem considered in [2] to the four-field model. Following [2,11,12] we define an initial force free bipolar vortex equilibrium state:

$$\psi^0(x,y)=\begin{cases}\left[2/kJ_0(k)\right]J_1(kr)\cos\theta, & r<1,\\ \left(r-1/r\right)\cos\theta, & r>1,\end{cases}\qquad J_1(k)=0 \tag{14a}$$

We have defined a polar coordinate system such that $y = r\cos\theta$, $x = r\sin\theta$. The initial toroidal field is defined as:

$$I^0(x,y)=\begin{cases}\sqrt{k^2\psi^2\left(x,y\right)+B_0^2} & r<1\\ B_0 & r>1\end{cases} \tag{14b}$$

It is readily verified that these satisfy the equilibrium condition:

$$\nabla^2\psi^0+\tfrac{1}{2}\frac{dI^{02}}{d\psi}=0. \tag{14c}$$

This equilibrium is known to be unstable to a tilting motion.

As in [2], the simulation box is a square with sides of length 4 that is divided into *(N-1) ×(N-1)* rectangular regions, each with two right triangles (using the diagonal that runs from upper right to lower left). Conducting, no slip boundary conditions are applied at the walls. Thus, at the y boundary, we impose:

$$\psi=\frac{\partial\psi}{\partial x}=\frac{\partial^2\psi}{\partial x^2}=0,\ I=\frac{\partial I}{\partial x}=\frac{\partial^2 I}{\partial x^2}=0, \tag{15}$$

$$V_z=\frac{\partial V_z}{\partial x}=\frac{\partial^2 V_z}{\partial x^2}=0,\ \phi=\frac{\partial\phi}{\partial x}=\frac{\partial^2\phi}{\partial x^2}=\frac{\partial\phi}{\partial y}=\frac{\partial^2\phi}{\partial x\partial y}=0,$$

with similar, but rotated boundary conditions applied at the x-boundary.

The baseline solution used uniform values of $\eta=\mu=0.001$, $h=2(\Delta x)^2$, $\nu=(\Delta x)^2\eta$. The instability is known to persist even at $\eta=0$ and is thus considered an ideal instability. To examine the effect of the Hall term on this mode, we specify a value of the ion skin depth $d_i$ and run the code in a linear mode to calculate the linear growth rate. Figure 1 gives this growth rate as a function of the square of $d_i$, for which it is seen to have a near linear dependence. Results for both $N=15$ and $N=31$ are shown, with those for $N=61$ being indistinguishable from the $N=31$. This study was performed with time-step $\Delta t=0.05$, but the growth rates changed by less than 2% when going from this value to $\Delta t=0.20$. The initial equilibrium and corresponding eigenmode for the case with $N=61$ and $d_i=0.2$ is shown in Fig. 2 (a)-(f) where we display contours of the equilibrium poloidal flux as well as perturbed values of the magnetic flux $\psi$, the current density $J \equiv \nabla^2\psi$, the stream function $\phi$, the z-directed magnetic field $I$, and the z-component of the velocity, $V_z$.

To determine the effect of the dissipation coefficients $h$ and $\nu$ on the solution, we have recomputed the configuration shown in Fig. 2 with a range of values of these. We find that if we write $h = C_1(\Delta x)^2$ and $\nu = C_2(\Delta x)^2\eta$, then we require $C_1 \geq 0.5$ and $C_2 \geq 0.5$ (approximately) for numerical stability. However, the computed growth rate increases by only 0.013% in varying $C_1$ in the range [0.5, 2.0], and by 0.53% when varying $C_2$ in this same range.

## VI. Harris Reconnection

We define a Harris equilibrium and perturbation similar to the one used in the Geospace Environmental Modeling (GEM) magnetic reconnection challenge [13], but within the limitations of the four-field equations. The initial equilibrium, shown in Fig. 3, is defined by an equilibrium and a perturbed magnetic flux function as follows:

$$\psi^0(x,y) = \frac{1}{2}\log(\cosh 2y); \qquad \psi(x,y) = \varepsilon \cos k_x x \cos k_y y \tag{16}$$

with all the other quantities initialized to zero. The initial equilibrium and perturbed current densities are just the Laplacian of the flux, $J^0 = \nabla^2\psi^0, J = \nabla^2\psi.$ The computation is carried out in a rectangular domain $-L_x/2 \le x \le L_x/2$ and $-L_y/2 \le y \le L_y/2$. The system is taken to be periodic in the x direction with ideal conducting boundaries, Eq. (15), at $y = \pm L_y/2$. As in [11], we chose the parameters such that $k_x = 2\pi/L_x$, $k_y = \pi/L_y$, with $L_x = 25.6, L_y = 12.8, \varepsilon = 0.1.$

We illustrate the results from a pair of comparison calculations in Figs. 3-7 . Both cases had $N=61$, $\eta=\mu=0.001$, $h=C_1(\Delta x)^2$, $\nu=C_2(\Delta x)^2\eta$, $C_1=4$, $C_2=1$, time step, $\Delta t=0.25$; and implicit parameter $\theta=0.6$. The first case had the ion skin depth set to zero, $d_i = 0$, while the second case had $d_i=1.0$.

Figures 4 and 5 show the poloidal magnetic flux (top) and current density (bottom) for the two cases at time $t=37.5$. We see in Fig. 4 that the case with $d_i = 0$ (resistive MHD) has a thin current layer on the midplane, known as the Sweet-Parker [14]layer. The corresponding case with $d_i=1.0$ (Hall-MHD) is shown in Figs. 5-6. In comparing Fig. 4 and Fig. 5, we see

that the Sweet-Parker layer is much shorter with $d_i=1$, and the reconnection region has essentially changed character from a Y-point to an X-point as expected[15]. In Fig. 6 we see the out of plane (z-directed) velocity (top) and magnetic field (bottom) in the Hall-reconnection case with $d_i=1$. Large in-out flows develop as a result of the reconnecting fields. The *z*-component of the magnetic field forms the characteristic quadrupole structure near the midplane.

We define the *reconnected magnetic flux* as: $\Psi(t) = \frac{1}{2}[\psi(0,0,t) - \psi(L_x/2,0,t)]$, and the *reconnection rate* as the time derivative of this. In Figure 7 we show a comparison of the amount of reconnected flux (dark curves) and the reconnection rates (red curves) vs time for the two cases, with several values of the hyper-dissipation coefficients for the $d_i=1.0$ case . It is seen that the Hall reconnection case with $d_i=1.0$ causes reconnection to occur about eight times faster than the resistive MHD case with $d_i=0$ for these parameters, and the results are relatively insensitive to the values of $C_1$ and $C_2$ as long as these are near unity. Varying $C_1$ in the range [0.75,1.25] or $C_2$ as in the range [2.0,4.0] each cause the maximum growth rate to increase by less than 1.5%, indicating that the solution is adequately converged in these parameters.

## VII. The Taylor Problem

The Taylor problem [3] consists of an initial magnetic field given by the flux function

$$\psi^0(y) = -\tfrac{1}{2}y^2 \tag{17}$$

The *z*-component of the magnetic field, $I^0(x,y)$ , is initially zero, as are the velocity variables $\phi^0$ and $V_z^0$ . For times $t \geq 0$ , the top and bottom boundaries are perturbed as follows:

$$\begin{aligned}\psi(x,\pm 1) &= \varepsilon(t)\cos(kx)\\ \phi(x,\pm 1) &= \mp\frac{1}{k}\dot{\varepsilon}(t)\sin(kx)\end{aligned} \tag{18}$$

The left and right boundaries are periodic. The time dependent perturbation function is defined as

$$\varepsilon(t) = \varepsilon^0\left[1-\left(1+t/\tau\right)\exp(-t/\tau)\right] \tag{19}$$

This problem has been studied both theoretically [16] and numerically [17] for the case of resistive MHD ($d_i=0$), but only numerical results [3] exist for the "two-fluid" or "Hall MHD" case of non-zero $d_i$.

The results of a series of calculations with $\varepsilon^0=.01,\ \tau=1.0,\ k=2\pi/L_x,\ \eta=\mu=10^{-4}$ ,$h=(\Delta x)^2,\ \nu=(\Delta x)^2\eta$ are presented in Fig. 8. The reconnected flux (top) and reconnection rate (bottom) vs. time are shown for different values of the collisionless ion skin depth $d_i$. The parameter $d_i$ is seen to have a significant impact on the reconnection rate, especially at early time. These results are seen to be qualitatively similar to Fig. 1 of Ref. [3], but extend those results to a nonlinear regime with a larger perturbation amplitude. More generally, the fact that $d_i$ ,or the Hall term, can greatly accelerate the rate of forced magnetic reconnection is consistent with results reported in earlier studies.

The calculations presented in Fig. 8 were performed on a domain with $L_x=8$, $L_y=2$, which was broken up into $60\times60$ rectangles, each divided into two triangles with a line from upper right to lower left. The other numerical parameters used were $\delta t=0.5$ and $\theta=0.6$. As in the other studies in this paper, there was no attempt to concentrate resolution in the reconnection layer, although this could dramatically increase the efficiency of this method and will be pursued in future studies.

## VIII. Summary and Discussion

A new technique for solving the extended MHD equations has been described and applied to the four-field model. This is a generalization of Appendix D of [2] where the MHD two-field model was discussed. The further generalization of this method to the fully compressible six-field or eight-field system of the full extended MHD equations is underway.

The method is characterized by representing the fluid and field in a potential/stream-function representation [1] in which higher derivatives occur. The higher derivatives are handled by using a compact triangular high-order finite element representation with $C^1$ continuity rather than by introducing auxiliary variables that would increase the rank of the matrices.

The split semi-implicit time advance is introduced which breaks the time advance into two steps each cycle. In the first step, the implicit method avoids time-step restrictions due to the Alfvén waves by inverting the ideal MHD force operator. In the second step, the implicit field advance avoids time-step restrictions due to the dispersive waves. It was shown in Sec. IV that the combined two-step time advance is unconditionally stable for arbitrary time step as long as the implicitness parameter $\theta$ is greater than ½. The relatively small matrices that need to be inverted make a direct sparse matrix inversion practical. A side benefit is that for linear problems, the LU decomposition only needs to be performed once, making the method exceptionally efficient.

The present work demonstrated the validity of this method by calculating the effects of the collisionless ion skin depth on the ideal MHD tilt mode, and on the rate of magnetic

reconnection for both a self-reconnecting and a forced reconnection system. Future work will extend this to a higher order system of equations, to toroidal geometry, and to three dimensions.

Finally we remark that we did not take advantage of the geometrical flexibility that is offered by triangles in the applications presented here. Triangular elements offer the potential to fit complex domain boundaries and to easily add refinement where needed. This will be exploited in future studies.

**Acknowledgements**

The authors benefited from many useful discussions with their colleagues: J. Chen, P. Fischer, G. Fu, W. Park, R. Samtaney, C. Sovinec, H. Strauss, and L. Sugiyama in particular. This work was supported by US DoE contract DE-AC02-76CH03073 and by the DOE SciDAC Center for Extended Magnetohydrodynamic Modeling.

**Appendix A: Definitions and symmetry relations.**

The matrix and tensor quantities used in the text are defined as follows. These are evaluated by closed form integration of the local polynomial expansions as described in Appendices B and D of [2].

$$D_{i,j}\Phi_j \equiv \iint v_i(\xi,\eta)\phi(\xi,\eta)d\xi d\eta$$

$$A_{i,j}\Phi_j \equiv \iint v_i(\xi,\eta)\nabla^2\phi(\xi,\eta)d\xi d\eta$$

$$B_{i,j}\Phi_j \equiv \iint v_i(\xi,\eta)\nabla^4\phi(\xi,\eta)d\xi d\eta$$

$$G_{i,j,k}\Psi_j\Phi_k \equiv \iint v_i(\xi,\eta)\left[\nabla^2\psi,\phi\right]d\xi d\eta = -G_{k,j,i}\Psi_j\Phi_k$$

$$K_{i,j,k}\Psi_j\Phi_k \equiv \iint v_i(\xi,\eta)\left[\psi,\phi\right]d\xi d\eta = -K_{i,k,j}\Psi_j\Phi_k$$

$$P_{i,j,k,l}\Psi_j\Phi_k Z_l \equiv \iint v_i(\xi,\eta)\left[\left[\phi,\nabla^2\psi\right],\zeta\right]d\xi d\eta = -P_{l,j,k,i}\Psi_j\Phi_k Z_l$$

$$(note: P_{k,j,i,l}\Psi_j\Phi_k Z_l = \iint v_i(\xi,\eta)\left[\nabla^2\psi,\left[\zeta,\phi\right]\right]d\xi d\eta = -P_{l,j,i,k}\Psi_j\Phi_k Z_l)$$

$$\begin{aligned} Q_{i,j,k,l}\Phi_j\Psi_k Z_l &\equiv \iint v_i(\xi,\eta)\left[\left[\phi,\psi\right],\zeta\right]d\xi d\eta = -Q_{i,k,j,l}\Phi_j\Psi_k Z_l \\ &= -Q_{l,j,k,i}\Phi_j\Psi_k Z_l = Q_{l,k,j,i}\Phi_j\Psi_k Z_l \end{aligned}$$

$$\begin{aligned} R_{i,j,k,l}\Phi_j\Psi_k Z_l &\equiv \iint v_i(\xi,\eta)\left\{\left[\left[\phi_x,\psi_x\right],\zeta\right]+\left[\left[\phi_y,\psi_y\right],\zeta\right]\right\}d\xi d\eta \\ &= -R_{l,j,k,i}\Phi_j\Psi_k Z_l = -R_{i,k,j,l}\Phi_j\Psi_k Z_l = R_{l,k,j,i}\Phi_j\Psi_k Z_l \end{aligned}$$

$$D_{i,j}J_j \equiv A_{i,j}\Psi_j$$

$$C^0_{i,j,k,l} \equiv \begin{bmatrix} P_{k,j,i,l} - P_{i,j,k,l} + P_{i,k,j,l} + 2R_{i,j,k,l} \\ P_{k,l,i,j} - P_{i,l,k,j} + P_{i,k,l,j} + 2R_{i,l,k,j} \end{bmatrix}$$

$$\bar{G}_{i,j,k} \equiv (G_{i,k,j} + G_{i,j,k})$$

$$\bar{Q}_{i,j,k,l} \equiv \tfrac{1}{2}\left(Q_{i,j,k,l} + Q_{i,j,l,k}\right)$$

## Appendix B: The Matrix Elements

Making use of the definitions and symmetry relations in Appendix A, the matrix elements are given as follows:

$$S_{11}^{\nu} = \begin{Bmatrix} A_{i,j} + \theta\delta t\left[-\mu B_{i,j} + \bar{G}_{i,j,k}(\Phi_k + \Phi_k^0)\right] \\ +(\theta\delta t)^2 C_{i,k,j,l}^0 \tfrac{1}{2}(\Psi_k + \Psi_k^0)(\Psi_l + \Psi_l^0) \end{Bmatrix}$$

$$S_{21}^{\nu} = \begin{Bmatrix} -\theta\delta t K_{i,j,k}(V_{zk} + V_{zk}^0) \\ -(\theta\delta t)^2 Q_{i,j,k,l}\left[(I_k + I_k^0)(\Psi_l + \Psi_l^0) - (\Psi_k + \Psi_k^0)(I_l + I_l^0)\right] \end{Bmatrix}$$

$$S_{22}^{\nu} = \begin{Bmatrix} D_{i,j} - \theta\delta t\left[\mu(A_{i,j} - hB_{i,j}) + K_{i,k,j}(\Phi_k + \Phi_k^0)\right] \\ -(\theta\delta t)^2 \bar{Q}_{i,j,k,l}(\Psi_k + \Psi_k^0)(\Psi_l + \Psi_l^0) \end{Bmatrix}$$

$$D_{11}^{\nu} = \begin{Bmatrix} A_{i,j} + \delta t(1-\theta)\mu B_{i,j} + \delta t\bar{G}_{i,j,k}\left[\theta(\Phi_k + \Phi_k^0) - (\tfrac{1}{2}\Phi_k + \Phi_k^0)\right] \\ +\theta(\theta-1)(\delta t)^2 C_{i,k,j,l}^0 \tfrac{1}{2}(\Psi_k + \Psi_k^0)(\Psi_l + \Psi_l^0) \end{Bmatrix}$$

$$D_{21}^{\nu} = \begin{Bmatrix} \delta t K_{i,j,k}\left[-\theta(V_{zk} + V_{zk}^0) + (\tfrac{1}{2}V_{zk} + V_{zk}^0)\right] \\ -\theta(\theta-1)(\delta t)^2 Q_{i,j,k,l}\left[(I_k + I_k^0)(\Psi_l + \Psi_l^0) - (\Psi_k + \Psi_k^0)(I_l + I_l^0)\right] \end{Bmatrix}$$

$$D_{22}^{\nu} = \begin{Bmatrix} D_{i,j} + \delta t\left[(1-\theta)\mu(A_{i,j} - hB_{i,j}) + K_{i,k,j}\left[(\tfrac{1}{2}\Phi_k + \Phi_k^0) - \theta(\Phi_k + \Phi_k^0)\right]\right] \\ -\theta(\theta-1)(\delta t)^2 \bar{Q}_{i,j,k,l}(\Psi_k + \Psi_k^0)(\Psi_l + \Psi_l^0) \end{Bmatrix}$$

$$R_{11}^{\nu} = \begin{Bmatrix} \delta t\bar{G}_{i,j,k}(\tfrac{1}{2}\Psi_k + \Psi_k^0) + \theta(\delta t)^2 \eta G_{i,k,j} J_k \\ +\theta(\delta t)^2 d_i C_{i,j,k,l}^0 \times\left[(I_k + I_k^0)(\tfrac{1}{2}\Psi_l + \Psi_l^0)\right] \end{Bmatrix}$$

$$R_{12}^{\nu} = \left\{\theta(\delta t)^2 d_i C_{i,k,j,l}^0 \times\left[\tfrac{1}{2}\Psi_k^0\Psi_l^0\right]\right\}$$

$$R_{21}^{\nu} = \begin{Bmatrix} -\delta t K_{i,j,k}(\tfrac{1}{2}I_k + I_k^0) \\ +\theta(\delta t)^2 \begin{pmatrix} -d_i\left[P_{i,j,k,l} + P_{i,k,j,l} + P_{i,l,k,j}\right]\times\left[\Psi_k^0\Psi_l^0 + \tfrac{1}{2}\left(\Psi_k\Psi_l^0 + \Psi_l\Psi_k^0\right) + \tfrac{1}{3}\Psi_k\Psi_l\right] \\ -d_i Q_{i,j,k,l}\left[I_k^0 I_l^0 + \tfrac{1}{2}\left(I_k I_l^0 + I_l I_k^0\right) + \tfrac{1}{3}I_k I_l\right] + \eta(G_{i,k,j} - G_{i,j,k})(\tfrac{1}{2}I_k + I_k^0) \end{pmatrix} \end{Bmatrix}$$

$$R_{22}^{\nu} = \begin{Bmatrix} +\delta t K_{i,j,k}(\tfrac{1}{2}\Psi_k + \Psi_k^0) \\ +\theta(\delta t)^2 \begin{pmatrix} \eta\left[(G_{i,j,k} - G_{i,k,j})(\tfrac{1}{2}\Psi_k + \Psi_k^0)\right] \\ \quad - d_i\left[Q_{i,k,j,l} + Q_{i,k,l,j}\right]\times\left[\Psi_k^0 I_l^0 + \tfrac{1}{2}\left(\Psi_k I_l^0 + I_l\Psi_k^0\right) + \tfrac{1}{3}\Psi_k I_l\right] \end{pmatrix} \end{Bmatrix}$$

$$S_{11}^{p} = \left\{ D_{i,j} - \theta\delta t \left[ \eta A_{i,j} - \nu B_{i,j} + K_{i,k,j}(\Phi_k + \Phi_k^0) + d_i K_{i,j,k}(I_k + I_k^0) \right] \right\}$$

$$S_{12}^{p} = -\theta\delta t d_i K_{i,k,j}(\Psi_k + \Psi_k^0)$$

$$S_{21}^{p} = -\theta\delta t \left[ d_i \bar{G}_{i,j,k}(\Psi_k + \Psi_k^0) + K_{i,k,j}(V_{zk} + V_{zk}^0) \right]$$

$$S_{22}^{p} = \left\{ D_{i,j} - \theta\delta t \left[ K_{i,k,j}(\Phi_k + \Phi_k^0) + \eta A_{i,j} - \nu B_{i,j} \right] \right\}$$

$$D_{11}^{p} = \left\{ D_{i,j} + \delta t \begin{bmatrix} (1-\theta)(\eta A_{i,j} - \nu B_{i,j}) + K_{i,k,j}\left[ -\theta(\Phi_k + \Phi_k^0) + \tfrac{1}{2}\Phi_k + \Phi_k^0 \right] \\ + d_i K_{i,j,k}\left[ -\theta(I_k + I_k^0) + \tfrac{1}{2} I_k + I_k^0 \right] \end{bmatrix} \right\}$$

$$D_{12}^{p} = \delta t d_i K_{i,k,j}\left[ -\theta(\Psi_k + \Psi_k^0) + \tfrac{1}{2}\Psi_k + \Psi_k^0 \right]$$

$$D_{21}^{p} = \delta t \begin{Bmatrix} d_i \bar{G}_{i,j,k}\left[ -\theta(\Psi_k + \Psi_k^0) + \tfrac{1}{2}\Psi_k + \Psi_k^0 \right] \\ + K_{i,k,j}\left[ -\theta(V_{zk} + V_{zk}^0) + \tfrac{1}{2} V_{zk} + V_{zk}^0 \right] \end{Bmatrix}$$

$$D_{22}^{p} = \left\{ D_{i,j} + \delta t \left[ K_{i,k,j} \left\{ -\theta(\Phi_k + \Phi_k^0) + \tfrac{1}{2}\Phi_k + \Phi_k^0 \right\} + (1-\theta)(\eta A_{i,j} - \nu B_{i,j}) \right] \right\}$$

$$R_{11}^{p} = \delta t \theta K_{i,j,k}(\Psi_k + \Psi_k^0)$$

$$R_{21}^{p} = \delta t \theta K_{i,j,k}(I_k + I_k^0)$$

$$R_{22}^{p} = \delta t \theta K_{i,j,k}(\Psi_k + \Psi_k^0)$$

$$Q_{11}^{p} = \delta t K_{i,j,k}\left[ -\theta(\Psi_k + \Psi_k^0) + \tfrac{1}{2}\Psi_k + \Psi_k^0 \right]$$

$$Q_{21}^{p} = \delta t K_{i,j,k}\left[ -\theta(I_k + I_k^0) + \tfrac{1}{2} I_k + I_k^0 \right]$$

$$Q_{22}^{p} = \delta t K_{i,j,k}\left[ -\theta(\Psi_k + \Psi_k^0) + \tfrac{1}{2}\Psi_k + \Psi_k^0 \right]$$

**References**


[1] W. Park, E. V. Belova, G. Y. Fu, *et al.*, Phys Plasmas **6,** Part 2, 1796-1803 (1999)

[2] S.C. Jardin, J. Comp. Phys. **200,** 133-152 (2004)

[3] R.Fitzpatrick, Phys Plasmas **11,** 937-946 (2004)

[4] R. Hazeltine, M. Kotschenreuther, P. Morrison, Phys. Fluids **28,** 2466 (1985)

[5] D. Biscamp, E. Schwarz, and J. F. Drake, Phys. Plasmas **4,** 1002 (1997)

[6] B. N. Rogers, R. E. Denton, J. F. Drake, and M. A. Shay, Phys. Rev. Lett., **87,** 19504 (2001)

[7] E. J. Caramana, J. Comp. Phys. **96,** 484-493 (1991)

[8] C. R. Sovinec, A. H. Glasser, G. A. Gianakon, *et al.*, J. Comput Phys. **195,** 355-386 (2004)

[9] D. Braess, "Finite Elements", (Cambridge University Press, 2001)

[10] J.W. Demmel, J.R. Gilbert, Y. S. Li, "SuperLU Users Guide", U.C. Berkeley, October 2003

[11] H. R. Strauss and D. W. Longcope, J. Comput. Phys, **147**, 318-336 (1998)

[12] R. Richard, R. D. Sydora, and M. Ashour-abdalla, Phys. Fluids B **2**, 488 (1990)

[13] J. Birn, J.F. Drake, M. A. Shay, *et al.*, Geophys. Res.:Space **106,** 3715 (2001)

[14] E. N. Parker, J. Geophys. Res. **62,** 509 (1957)

[15] D. Biskamp, E. Schwarz, J. F. Drake, Phys. Plas. **4,** 1002 (1997)

[16] T. S. Hahm and R. M. Kulsrud, Phys. Fluids **28**, 2412 (1985)

[17] R. Fitzpatrick, Phys. Plasmas **10**, 1782 (2003)

**Figure 1**: Dependence of the linear growth rate for the tilt mode on the square of the ion skin depth, $d_i^2$ Results are shown for calculations with 15×15 and 31×31 rectangles, each divided into 2 triangles.

**Figure 2**: Linear eigenmodes for one of the calculations performed for Fig. 1 with *N=61* and $d_i=0.2$ . Shown are contours of (a) the equilibrium magnetic flux, $\Psi^0$; (b) the perturbed values of the magnetic flux, $\psi$; (c) the perturbed current density, J;(d) z-directed magnetic field, I; (e) the stream function, $\phi$; and (f) the z-component of the velocity, $V_{z,}$. The region (-1.5,1.5) × (-1.5,1.5) is shown while the calculation was performed on a (-2.0,2.0) × (-2.0,2.0) domain with conductor boundary conditions imposed.

**Figure 3:** Initial equilibrium poloidal magnetic flux $\psi$ (top) and current density J (bottom) for the Harris reconnection problem.

**Figure 4:** Poloidal magnetic flux (top) and current density (bottom) for the "resistive MHD" reconnection at time $t=37.5$ with $d_i=0$.

**Figure 5:** Poloidal magnetic flux (top) and current density (bottom) for the "Hall- MHD" reconnection at time $t=37.5$ with $d_i=1.0$.

**Figure 6**: Out of plane (*z*-directed) velocity (top) and magnetic field in the Hall-reconnection case with $d_i=1$ (bottom). Large in-out flows develop as a result of the reconnecting fields. The *z*-component of the magnetic field forms the characteristic quadrupole structure near the midplane.

**Figure 7:** Comparison of the amount of reconnected flux (dark curves) and the reconnection rates (red curves) vs time for the two cases. Three runs are shown for the $d_i=1$ case with $C_1=1, C_2=2$ (dashed), $C_1=1, C_2=4$ (dashed), $C_1=0.75, C_2=4$ (dashed-dotted). The reconnected flux and reconnection rate are essentially independent of these dissipation parameters over this range.

**Figure 8:** Reconnected flux (top) and reconnection rate (bottom) vs time for the Taylor problem for different values of the collisionless ion skin depth $d_i$. Other physical parameters were $\eta=\mu=10^{-4,}$ $h=(\Delta x)^2$ The parameter $d_i$ is seen to have a significant impact on the reconnection rate, especially at early time.

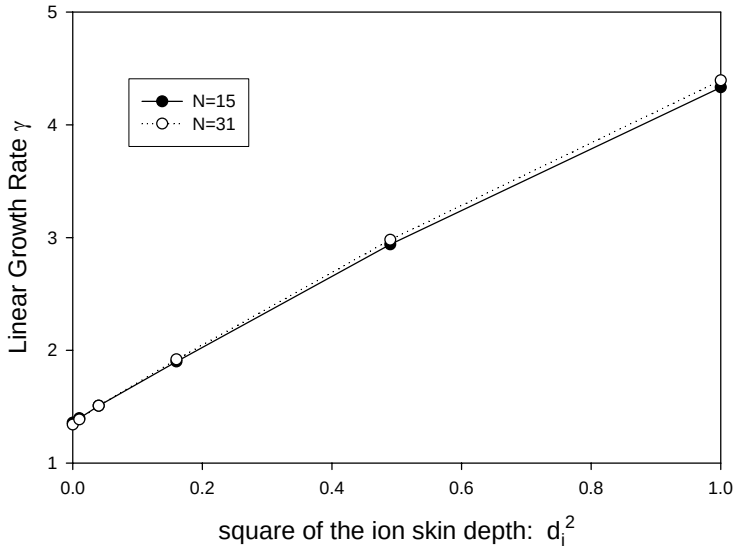
N=15
N=31
Linear Growth Rate γ
square of the ion skin depth: $d_i^2$
1
2
3
4
5
0.0
0.2
0.4
0.6
0.8
1.0

Figure 1

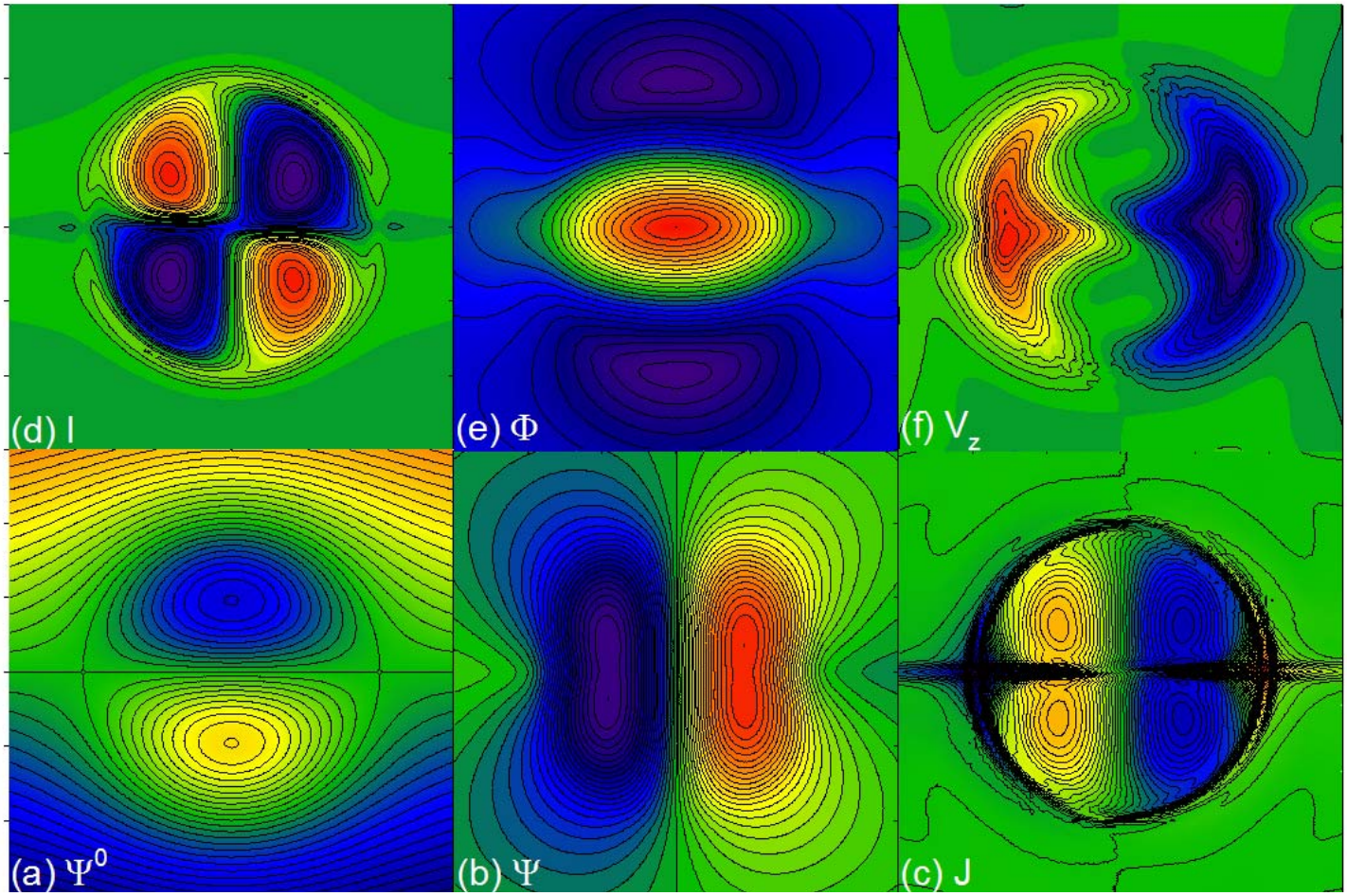


Figure 2

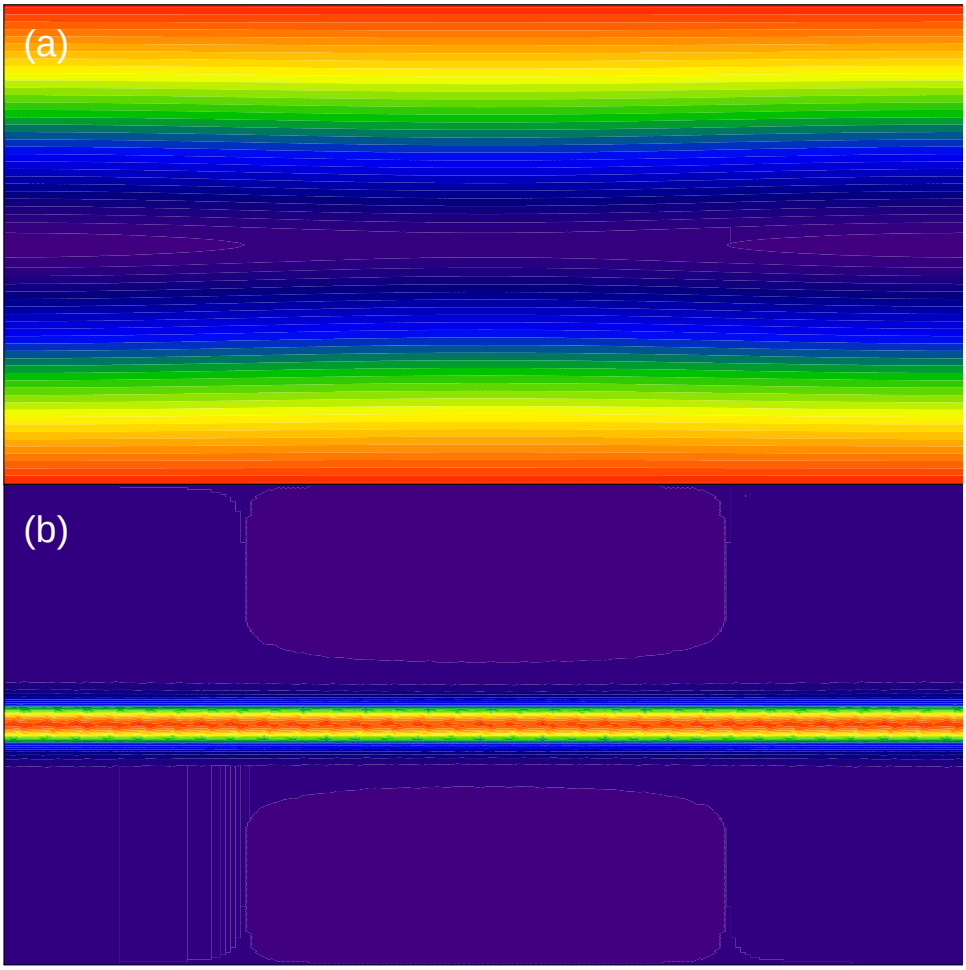


Figure 3

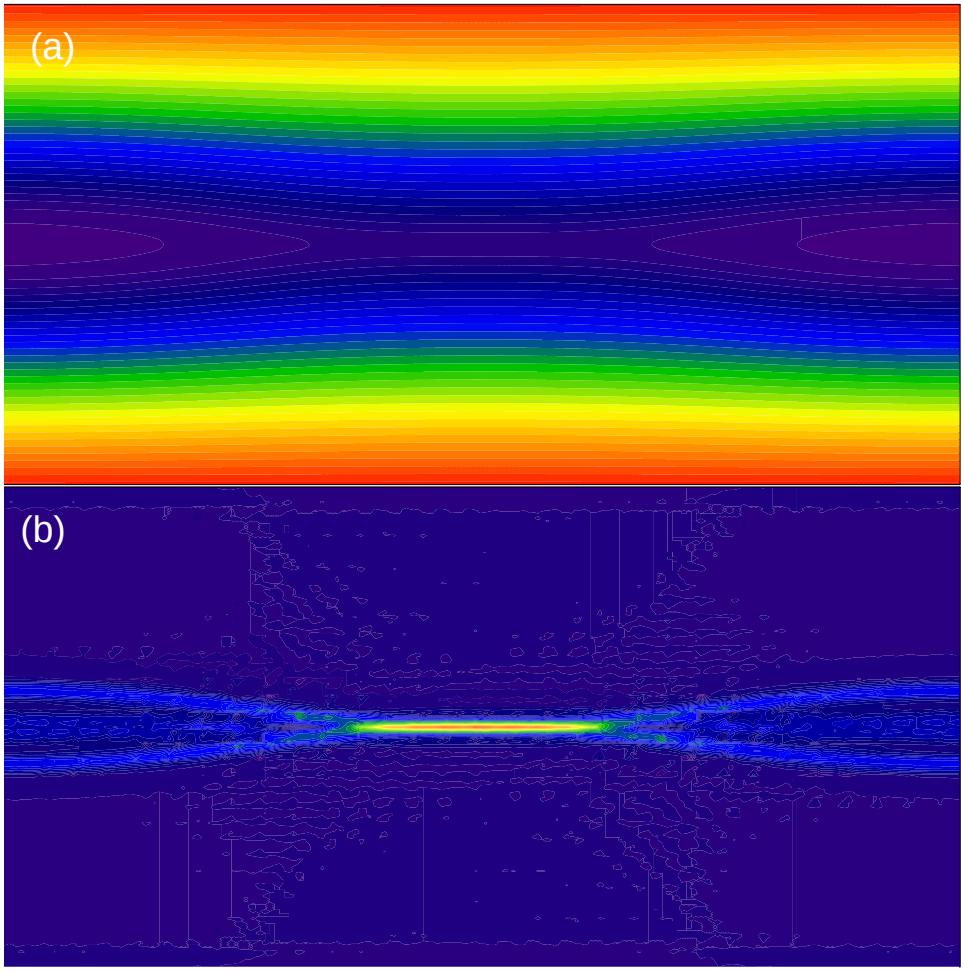


Figure 4

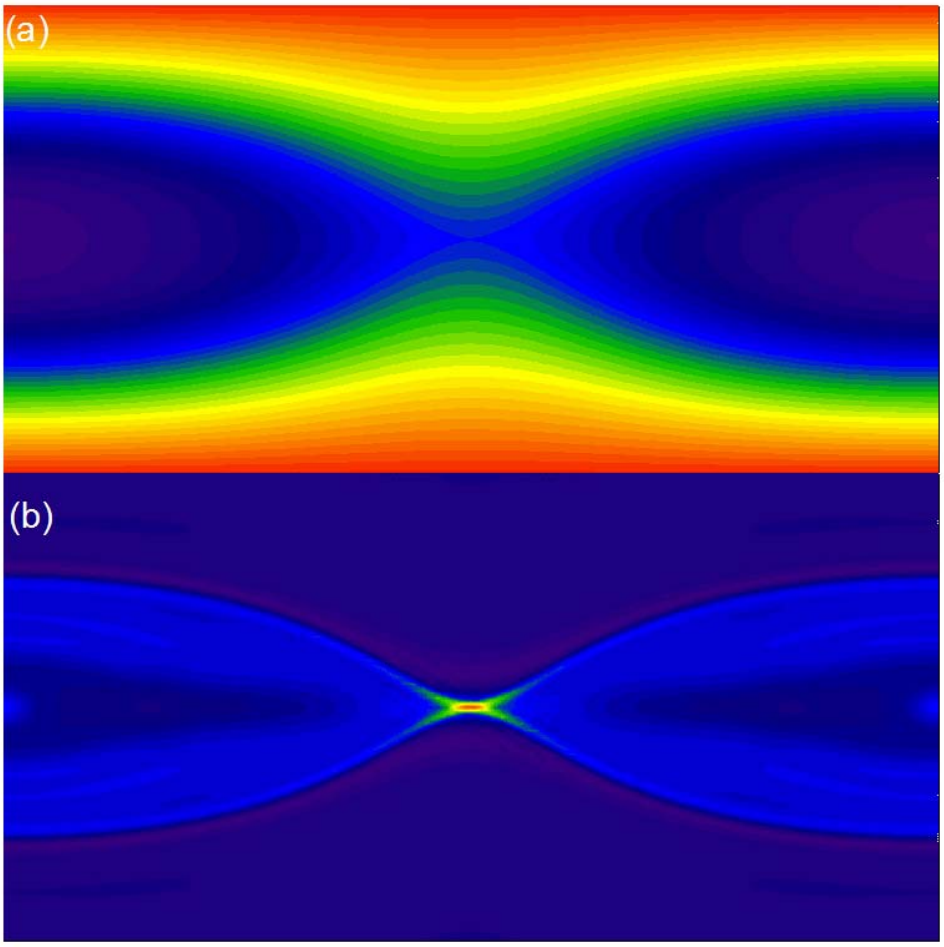


Figure 5

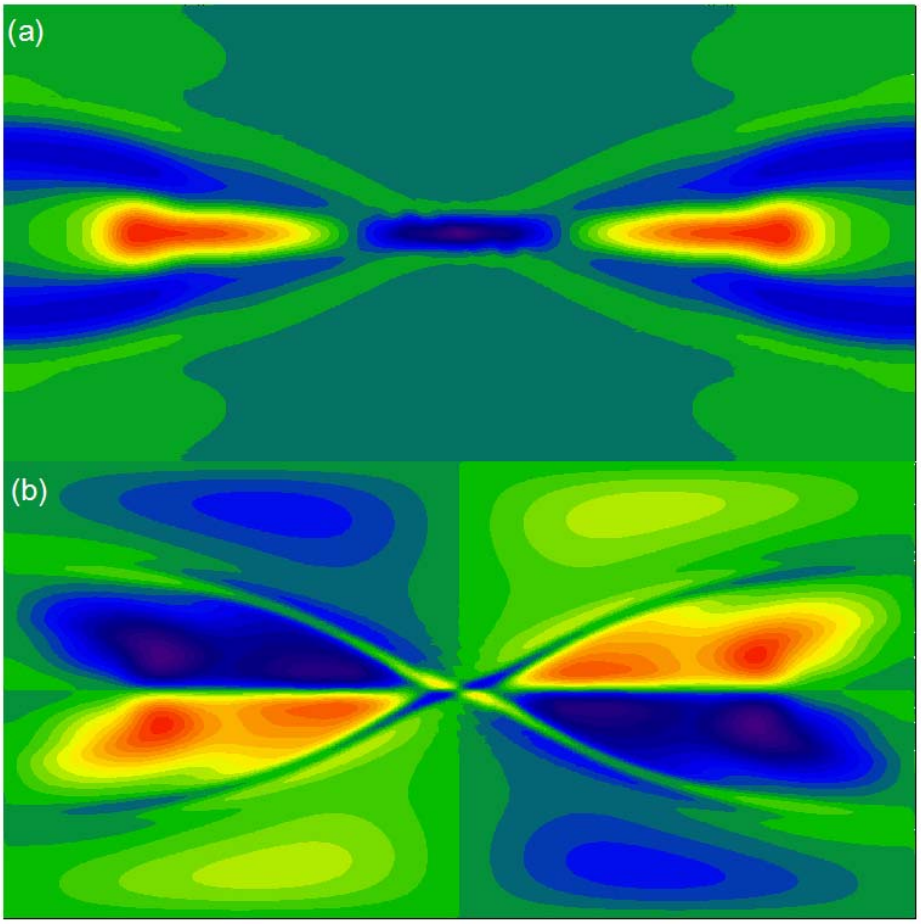


Figure 6

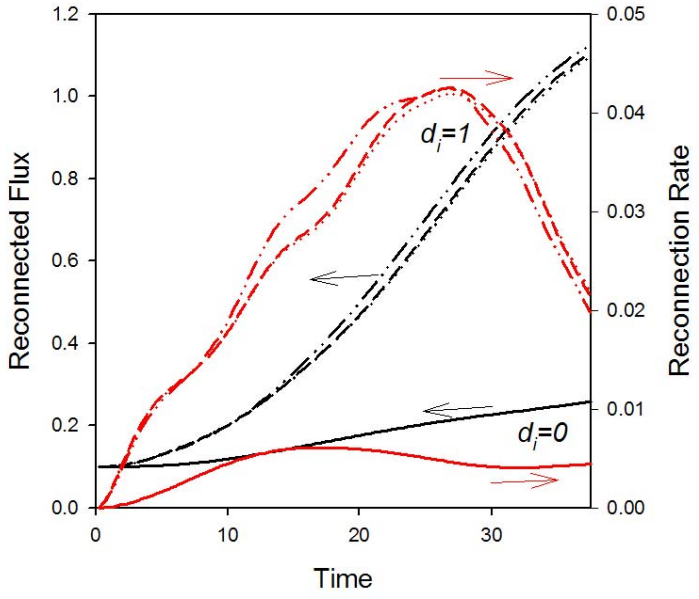
Reconnected Flux
Reconnection Rate
Time
$d_i$=1
$d_i$=0
0.0
0.2
0.4
0.6
0.8
1.0
1.2
0.00
0.01
0.02
0.03
0.04
0.05
0
10
20
30

Figure 7

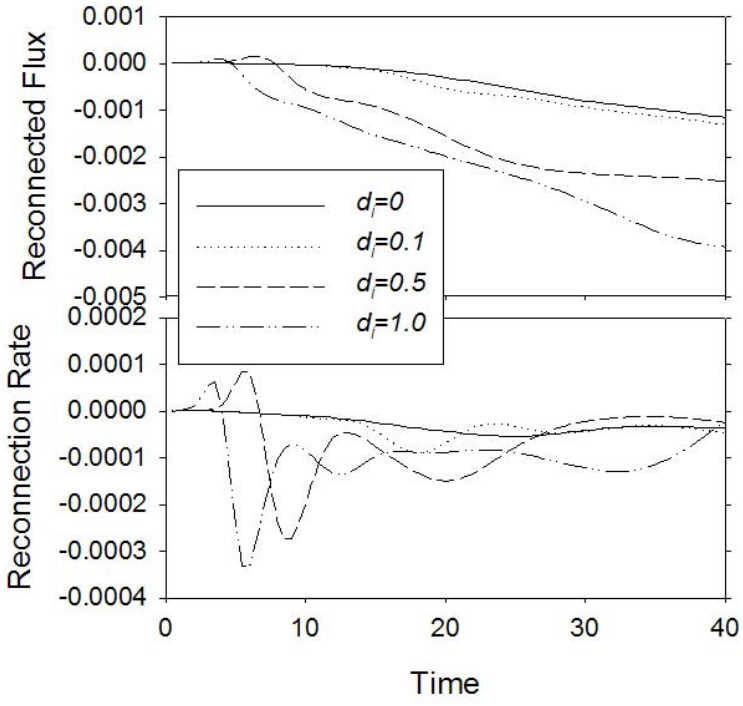
Reconnected Flux
Reconnection Rate
Time
$d_i$=0
$d_i$=0.1
$d_i$=0.5
$d_i$=1.0
0.001
0.000
-0.001
-0.002
-0.003
-0.004
-0.005
0.0002
0.0001
0.0000
-0.0001
-0.0002
-0.0003
-0.0004
0
10
20
30
40

Figure 8

## External Distribution

Plasma Research Laboratory, Australian National University, Australia

Professor I.R. Jones, Flinders University, Australia

Professor João Canalle, Instituto de Fisica DEQ/IF - UERJ, Brazil

Mr. Gerson O. Ludwig, Instituto Nacional de Pesquisas, Brazil

Dr. P.H. Sakanaka, Instituto Fisica, Brazil

The Librarian, Culham Laboratory, England

Mrs. S.A. Hutchinson, JET Library, England

Professor M.N. Bussac, Ecole Polytechnique, France

Librarian, Max-Planck-Institut für Plasmaphysik, Germany

Jolan Moldvai, Reports Library, Hungarian Academy of Sciences, Central Research Institute for Physics, Hungary

Dr. P. Kaw, Institute for Plasma Research, India

Ms. P.J. Pathak, Librarian, Institute for Plasma Research, India

Ms. Clelia De Palo, Associazione EURATOM-ENEA, Italy

Dr. G. Grosso, Instituto di Fisica del Plasma, Italy

Librarian, Naka Fusion Research Establishment, JAERI, Japan

Library, Laboratory for Complex Energy Processes, Institute for Advanced Study, Kyoto University, Japan

Research Information Center, National Institute for Fusion Science, Japan

Dr. O. Mitarai, Kyushu Tokai University, Japan

Dr. Jiangang Li, Institute of Plasma Physics, Chinese Academy of Sciences, People's Republic of China

Professor Yuping Huo, School of Physical Science and Technology, People's Republic of China

Library, Academia Sinica, Institute of Plasma Physics, People's Republic of China

Librarian, Institute of Physics, Chinese Academy of Sciences, People's Republic of China

Dr. S. Mirnov, TRINITI, Troitsk, Russian Federation, Russia

Dr. V.S. Strelkov, Kurchatov Institute, Russian Federation, Russia

Professor Peter Lukac, Katedra Fyziky Plazmy MFF UK, Mlynska dolina F-2, Komenskeho Univerzita, SK-842 15 Bratislava, Slovakia

Dr. G.S. Lee, Korea Basic Science Institute, South Korea

Institute for Plasma Research, University of Maryland, USA

Librarian, Fusion Energy Division, Oak Ridge National Laboratory, USA

Librarian, Institute of Fusion Studies, University of Texas, USA

Librarian, Magnetic Fusion Program, Lawrence Livermore National Laboratory, USA

Library, General Atomics, USA

Plasma Physics Group, Fusion Energy Research Program, University of California at San Diego, USA

Plasma Physics Library, Columbia University, USA

Alkesh Punjabi, Center for Fusion Research and Training, Hampton University, USA

Dr. W.M. Stacey, Fusion Research Center, Georgia Institute of Technology, USA

Dr. John Willis, U.S. Department of Energy, Office of Fusion Energy Sciences, USA

Mr. Paul H. Wright, Indianapolis, Indiana, USA

The Princeton Plasma Physics Laboratory is operated
by Princeton University under contract
with the U.S. Department of Energy.

Information Services
Princeton Plasma Physics Laboratory
P.O. Box 451
Princeton, NJ 08543

Phone: 609-243-2750
Fax: 609-243-2751
e-mail: pppl_info@pppl.gov
Internet Address: http://www.pppl.gov